A small molecule activator of kinesin-1 drives remodeling of the microtubule network

Thomas S. Randall[1], Yan Y. Yip[1], Daynea Wallock-Richards[1], Karin Pfisterer[1], Anneri Sanger[1], Weronika Ficek[1], Roberto A. Steiner[1], Andrew J. Beavil[1], Maddy Parsons[1] and Mark P. Dodding[1,2]*

[1] Randall Centre for Cell for Molecular Biophysics, King's College London, London, SE1 1UL, United Kingdom

[2] School of Biochemistry, University of Bristol, BS9 1TD, United Kingdom

*Correspondence to: mark.dodding@bristol.ac.uk

Abstract

The microtubule motor kinesin-1 interacts via its cargo-binding domain with both microtubules and organelles, and hence plays an important role in controlling organelle transport and microtubule dynamics. In the absence of cargo, kinesin-1 is found in an autoinhibited conformation. The molecular basis of how cargo engagement affects the balance between kinesin-1's active and inactive conformations and roles in microtubule dynamics and organelle transport is not well understood. Here we describe the discovery of kinesore, a small molecule that in vitro, inhibits kinesin-1 interactions with short linear peptide motifs found in organelle specific cargo adaptors, yet activates kinesin-1's function of controlling microtubule dynamics in cells, demonstrating that these functions are mechanistically coupled. We establish a proof-of-concept that a microtubule motor-cargo interface and associated autoregulatory mechanism can be manipulated using a small molecule, and define a new target for the modulation of microtubule dynamics.

Significance

Here we identify kinesore, as a cell permeable small molecule modulator of the kinesin-1 microtubule motor. Kinesore acts through the cargo binding domain of the motor to activate its function in controlling microtubule dynamics. Our chemical biology approach to understanding microtubule motor protein function provides new mechanistic insight into how this poorly understood activity of the motor is regulated and establishes a proof-of-concept that a microtubule motor-cargo interface and associated autoregulatory mechanism can be manipulated using a small molecule. In doing so, we define a new target for the modulation of microtubule dynamics. We suggest that this offers a new conceptual approach to consider for the chemical manipulation of the cytoskeleton and its motor proteins.

\body

Introduction

The heterotetrameric kinesin-1 microtubule motor plays a crucial role in spatial organization of many subcellular components by virtue of its capacity to transport diverse protein and ribonuclear protein complexes, vesicles and organelles on microtubules (1-4). Kinesin-1 also regulates the organization of the microtubule network itself, through its ability to mediate microtubule-microtubule interactions that result in their bundling and sliding (5-9). This activity is important for cytoplasmic streaming in drosophila oocytes, formation of microtubule based cellular processes and axonal regeneration (5, 10). These diverse functions rely on a capacity to translocate with high processivity towards the plus(+)end of microtubules imparted by the microtubule binding amino terminal ATPase motor domains of the dimeric kinesin heavy chains (KHCs) and a multivalent cargo binding domain comprised of the C-terminal domains of the KHCs and the kinesin light chains (KLCs), which contain binding sites for both organelle-specific cargo adaptors and microtubules (9, 11-15).

In the absence of cargo, kinesin-1 is in an autoinhibited, folded conformation that is stabilized by the interaction of a single C-terminal KHC tail with the motor domain dimer interface, thereby crosslinking the two motor domains and preventing futile cycles of ATP hydrolysis (16-22). We have recently shown that the KLCs, which regulate kinesin-1 activity (23, 24), also engage, in cis, in a second autoinhibitory intramolecular interaction between their tetratricopeptide repeat domain (KLC^{TPR}) and a negatively charged unstructured linker region immediately preceding it carrying a leucine-phenylalanine-proline (LFP) motif (25). Binding of organelle-specific cargo adaptors containing 'W-acidic' short-linear-peptide motifs to KLC^{TPR}, which can initiate kinesin-1 activation (11, 26, 27), displaces this intramolecular interaction causing a conformational change within the KLCs (25). We proposed that this cargo dependent conformational change acts a molecular switch to control the activity of the holoenzyme (25). We also recently provided evidence to suggest that one consequence of W-acidic motif engagement of KLC^{TPR} is to make a cargo binding site in the KHC tail, that is inaccessible in the autoinhibited conformation, available to bind cargo (28). The predominantly basic series of amino acids comprising this site can interact with closely related cargo adaptors sequences to stabilize the kinesin-1-cargo interaction and interestingly, is also known to interact with microtubules in an ATP-independent manner (9, 14, 15, 19). Collectively, these data suggest a stepwise model for kinesin-1 activation, in which engagement of KLC^{TPR} and resulting light chain conformational change, is the key upstream signal to activate kinesin-1, and, in a context dependent manner, results in either organelle transport, if KHC interacts with an organelle cargo adaptor(28), or microtubule bundling and sliding, if KHC interacts with microtubules. In support of such a proposition, the KLCs have been demonstrated to modulate the affinity of the KHC-tail for microtubules in a manner dependent on the KLC LFP-acidic linker region (24), and the W-acidic

motif containing kinesin-1 adaptor calsyntenin-1 was recently shown to play a role in regulating microtubule organization in dendritic arbor development (29). One prediction of such a model is that if kinesin-1 were to be activated under conditions where its capacity to interact with organelles was limited, its role in microtubule sliding and bundling would be promoted.

We employed a chemical biology based approach to test this hypothesis, seeking to identify small molecules that could induce KLC^{TPR} dependent kinesin-1 activation in the absence of organelle cargo adaptor engagement. This resulted in the identification of a compound that we have named kinesore, which in vitro, inhibits the interaction of KLC^{TPR} with the W-acidic lysosomal cargo adaptor SKIP. We show that in cells, kinesore induces the light chain conformational switch in a similar manner to activating cargo and causes the large-scale kinesin-1 dependent remodeling of the microtubule network. Thus, we demonstrate that the organelle transport and microtubule sliding/bundling functions of the motor are coupled through a shared activation mechanism. Moreover, we establish a proof-of-concept that a microtubule motor-cargo interface and associated autoregulatory mechanism can be manipulated using a small molecule, and offer an unexpected new target for the modulation of microtubule dynamics.

Results

Identification of kinesore as a small molecule inhibitor of the KLC2 - SKIP interaction

To identify small molecules that could induce KLC^{TPR} dependent kinesin-1 activation in the absence of organelle cargo adaptor engagement, we focused on the interaction between autoinhibited $aiKLC2^{TPR}$ (KLC2 161-480, *previously designated* $KLC2^{extTPR}$) and a W-acidic motif peptide from the lysosomal cargo adaptor SKIP ($SKIP^{WD}$) (25). Inclusion of the autoinhibitory N-terminal sequence on $KLC2^{TPR}$ results in an approximate 8-fold reduction in binding affinity (K_D increases to ≈8 μM from ≈1 μM). To bind $KLC2^{TPR}$, $SKIP^{WD}$ displaces this autoinhibitory interaction (25). Thus, one possible mechanism for the small molecule mediated inhibition of the SKIP-$aiKLC2^{TPR}$ interaction would be for a compound to act in a similar fashion to SKIP by displacing the intramolecular interaction to occupy the SKIP binding site, thus potentially mimicking SKIP induced activation whilst simultaneously inhibiting SKIP binding. This formed the rationale for a high-throughput small molecule screen.

We developed a primary in vitro time-resolved (TR) FRET assay (Figure 1A, top) coupled to a secondary fluorescence polarization (FP) based assay (Figure 1A, middle) to identify compounds that had the capacity to inhibit the interaction between $aiKLC2^{TPR}$ and $SKIP^{WD}$ and screened the 2908 compound Chemogenomic Library provided by Pfizer (see *materials and methods* for details). A tertiary FP screen of compounds from the Hit-2-Lead library (Chembridge), informed by this dataset, resulted in the

identification of 3,5-dibromo-N'-{[2,5-dimethyl-1-(3-nitrophenyl)-1H-pyrrol-3-yl]methylene}-4-hydroxybenzohydrazide, hereafter named *kinesore* (Figure 1A, bottom).

Consistent with its ability to target the kinesin-1-cargo interface, in pull down assays, kinesore inhibited the interaction between purified recombinant GST-SKIP(1-310) and full length haemaglutinin(HA)-KLC2 with a 50% reduction in binding at 12.5μM and elimination of any detectable binding at a 25μM kinesore (Figure 1B). In FP assays, kinesore inhibited the interaction of TAMRA-SKIP^{WD} with aiKLC2^{TPR} in a concentration dependent manner (Figure 1C) (30). Based upon this activity profile, and penetrant cellular phenotype described below, we decided to pursue it further. To the best of our knowledge, this compound has not been characterised before in any other context.

Kinesore remodels the microtubule network

To examine the effect of kinesore in cells, HeLa cells were treated with 50μM kinesore for one hour. As SKIP mediates the kinesin-1 dependent transport of late endosomes(LE)/lysosomes on microtubules (31), cells were immunostained for β-tubulin and LAMP1 (LE/lysosomes). In control conditions, as expected, lysosomes were distributed throughout the cytoplasm, with some peripheral and perinuclear clusters, in association with the characteristic radial microtubule array typically observed in this cell type (Figure 2A, top). Remarkably, in kinesore-treated cells, the microtubule network was entirely reorganized into a series of loops and bundles (Figure 2A, bottom). In addition, the lysosomal compartment accumulated in a juxta-nuclear position where there were relatively few microtubules. At 50μM kinesore, this phenotype was highly penetrant with 95±2.4% (n=3, total of 200 cells) of cells exhibiting a reorganized non-radial microtubule network. This phenotype emerged progressively with prominent loops and bundles in most cells becoming apparent after 30-35 minutes of treatment (Figure S1). In titration experiments, in cells treated for one hour, this phenotype became apparent at a concentration of 25μM kinesore, with relatively little effect at or below concentrations of 12.5μM (Figure S2A). The effect was reversible because a two hour washout of kinesore from cells treated for one hour led to the reestablishment of the radial microtubule array (Figure S2B), suggesting that this effect was not due to acute toxicity of the compound.

To examine the dynamic behavior of the reorganized microtubule network, HeLa cells stably expressing GFP-α-tubulin were treated with kinesore for one hour and imaged live. This revealed that the loops/bundles of microtubules, particularly in the cell periphery, were highly dynamic and engaged in complex microtubule-microtubule interactions (Figure 2B,C, supplementary movie 1). This phenotype is highly reminiscent of cells that overexpress the microtubule sliding Drosophila kinesin-14 family motor, Ncd, and so we considered this to be consistent with our hypothesis (32). Occasionally, cells also extended microtubule-based projections (Figure 2D, supplementary movie 1). Treatment of cells stably expressing the +end binding protein EB3 fused to red fluorescent protein (RFP) showed that whilst

microtubules +ends remained highly dynamic, the spatial organization and directionality of EB3 comets appeared disordered compared to control cells (Figure 2E, supplementary movies 2-4). Treatment of cells with 10μM nocodazole disrupted kinesore induced loops and bundles (Figure S3).

This kinesore-induced reorganization of the microtubule network was observed in a panel of mammalian normal and cancer cell lines, and thus was not restricted to HeLa cells (Figure S4). To our knowledge, this cellular phenotype does not closely resemble that of any known microtubule targeting agents that act directly upon tubulin, and consistent with this, kinesore did not significantly affect the kinetics of microtubule assembly in in vitro polymerization reactions and microtubules polymerized in the presence of kinesore were equally susceptible to cold induced destabilization. (Figure S5).

Kinesore induced remodeling of the microtubule network is dependent on kinesin-1

Next, we examined the effect of kinesore on cells overexpressing kinesin-1. In control cells transfected with Citruline (mCit)-tagged KHC (Kif5C) and HA-tagged KLC (KLC2), which form a complex when overexpressed(28), kinesin-1 displayed a predominantly diffuse localization and the microtubule network appeared substantially normal (Figure 3A, left). Consistent with an activation-like effect upon kinesin-1, in kinesore treated cells, KHC and KLC accumulated at the cell periphery (Figure 3A, right). In addition, the morphology of the kinesore-remodeled microtubule network was altered. Intracellular loops were less prominent, but instead cells showed large numbers of microtubule-rich projections emanating from the cell periphery. Structured illumination microscopy (SIM) imaging confirmed that kinesin-1 (KHC and KLC) associated with tubulin at the cell periphery in kinesore-treated cells (Figure 3B). We also noted their accumulation at the tip of a subset of microtubule rich projections (Figure 3B). Collectively, these data suggest that, as kinesore alters the localization of kinesin-1, and high expression of kinesin-1 modifies the kinesore-microtubule phenotype, kinesore likely acts upon kinesin-1. Consistent with this, fluorescent protein-labeled kinesin-1 subunits expressed under control of their endogenous promoter in HeLa-Kyoto cells (33), which display a predominantly diffuse localization under control conditions, associated with kinesore-induced microtubule loops and bundles (Figure S6). Similarly, when these cells (GFP-Kif5B) were lysed in a microtubule stabilizing buffer, kinesore increased the amount of KHC associated with a microtubule containing pellet fraction following sedimentation (Figure S7), without affecting the amount of tubulin in the pellet.

Formally testing the kinesin-1 dependence of kinesore induced remodeling of microtubules is complicated by the multiple genes that can encode KHC (Kif5A, Kif5B, Kif5C) and KLC (KLC1, KLC2, KLC3, KLC4) which have distinct cell and tissue expression profiles and which have the potential to undergo compensatory changes in expression following loss of a specific isotype (34). To address this, we used the commercially available KHC (KIF5B) CRISPR knockout, chronic myeloid leukemia (CML)

derived HAP1 cell line, and matched wild type control. In wild type HAP1 cells, transcriptomic data suggest that Kif5B is the predominant isotype at 61 transcripts per million (TPM). Kif5C is present at 21 TPM whilst Kif5A is not expressed (35). Consistent with this, Kif5B was detected in wild type cell extracts using a Kif5B-specific polyclonal antibody, but was absent in Kif5B KO cells. In contrast, pan-KHC antibody revealed a substantial but not complete reduction in total KHC expression, suggesting the presence of lower levels of another isotype (Figure 3C). In wild type cells, 50μM kinesore induced the remodeling of the microtubule network and the formation of extensive microtubule-rich projections. This phenotype was strongly suppressed in Kif5B knockout cells, confirming that microtubule remodeling induced by kinesore is dependent upon the presence of kinesin-1.

Kinesore induces the light chain conformational switch

These data suggest that kinesore, by engaging the KLC^{TPR} in a manner that inhibits interactions of kinesin-1 with activating cargo adaptors, may act in a 'cargo-mimetic' manner to promote kinesin-1 activation. To test this hypothesis, we employed our previously validated KLC conformation biosensor (Figure 4A) (25). In the absence of exogenous cargo, this biosensor reports a high FRET state consistent with a compact KLC conformation (FRET efficiency 15.77±0.76%). FRET is reduced by co-expression of the cytoplasmic domain of the W-acidic cargo adaptor CSTN1 (5.82±1.02%) (Figure 4B) (25), consistent with the notion that cargo binding by KLC^{TPR} results in conformational change in KLC. Treatment of cells with 50μM kinesore caused a comparable reduction in FRET (4.04±0.49%), suggesting that kinesore induces the light chain conformational switch in a manner similar to activating cargoes.

Discussion

Kinesin family proteins play key roles in both cargo transport on microtubules and in controlling microtubule dynamics to support a wide range of cellular processes (3, 36). Some, such as the kinesin-4 family member Kif21B possess both of these capacities which are fine tuned for its function (37). Is has been appreciated for many years that kinesin-1 also possesses both of these abilities (6). However, the molecular mechanisms that underpin and regulate the balance between these two activities and their relationship to kinesin-1 autoinhibition remain largely unknown. Here we have employed a chemical biology driven approach to test the hypothesis that these functions are linked though a common regulatory mechanism. Our identification of kinesore as a small molecule that inhibits the SKIP-KLC2 interaction in vitro yet promotes kinesin-1 function in controlling the organization of the microtubule network in cells strongly supports our hypothesis. Moreover, the data provides proof-of-concept that a microtubule motor-cargo interface and associated autoregulatory mechanism can be manipulated using a small molecule, and defines a potential new target for the modulation of microtubule dynamics.

Collectively, our data suggest a model in which kinesore engages the KLCs of kinesin-1 in cargo-like fashion to initiate crucial events in cargo-dependent activation, the net result of which is to promote the function of the motor in regulating microtubule bundling and sliding, leading to the remodeling of the microtubule network

Our favored model builds upon our recent studies (11, 25, 28) and of others (24, 26) and proposes that in the absence of cargo, kinesin-1 is in its 'double autoinhibited' conformations mediated by an intramolecular motor domain–KHC-tail interaction and the KLC^{TPR}–LFP-acidic linker interaction. Kinesin-1 activation is initiated by cargo binding to KLC^{TPR} resulting in displacement of the LFP-acidic linker region and light chain conformational change, which in turn leads to destabilization of KHC autoinhibition through a mechanism involving both steric and electrostatic factors (24, 25). One consequence of this is to make accessible a binding site in KHC-tail adjacent to the autoinhibitory IAK sequence. This site is capable of interacting with either organelle cargo adaptors (28) or microtubules (9, 14, 15, 19). Thus, the KLCs gate access to this crucial KHC-tail site. We suggest that kinesore initiates this process whilst simultaneously inhibiting KLC^{TPR} association with organelle cargo adaptors, forcing kinesin-1 to perform its role in promoting bundling and sliding, resulting in the formation of loops and bundles that bear a notable resemblance to those previously observed following over-expression of an active microtubule sliding kinesin-14 family member (32). Bundling of parallel microtubules and sliding of antiparallel microtubules (6) in the background of continuing + end dynamics progressively leads to the emergence of the complex phenotypes observed.

It is worth stating explicitly that we make no claim regarding the specificity of kinesore outside of this limited functional space. Given that the compound must be used at relatively high concentrations in cells (25 - 50μM) it is highly likely that other cellular targets exist, although it is unlikely that these make a significant contribution to the microtubule phenotype described. We have not observed any direct effects in vitro on tubulin polymerization suggesting that this not likely a major component of the cellular activity of kinesore, however, we cannot rule out the possibility of a synergistic direct or indirect activity that combines with the compound's effect on kinesin-1, that is not captured in these assays.

Nonetheless, it is worth reflecting on the proof-of-concept established here. To our knowledge this is the first time that the cargo-binding interface and associated autoregulatory mechanism of a cytoskeletal motor has been targeted using a small molecule. We suggest that this offers several exciting possibilities for the future. Most small molecules that modulate cytoskeletal motor protein function target the ATPase activity or motility mechanisms associated with motor domains that are relatively well conserved within the kinesin, myosin and dynein families, thus hindering the development of specific functional modulators. In contrast, although autoregulation coupled to cargo recognition represent common themes, the mechanisms by which this is achieved are quite divergent (3, 38-41). For example, kinesin-1 is the

only kinesin family member that employs a TPR domain–short linear motif cargo recognition mechanism (11) which is coupled to its autoregulatory mechanism (25). Indeed, this makes it very unlikely that kinesore has activity against any other kinesin family member. Thus, targeting of these mechanisms may represent a novel approach to achieving small molecule control of motor protein function for use as both research tools and for potential therapeutic purposes where motor proteins are dysregulated. Importantly, this approach offers the prospect of not only inhibiting, but also enhancing specific motor protein activities. Developments over recent years establishing the structural basis for cargo recognition and autoregulation are an essential prerequisite for this approach: myosin V, MCAK, cytoplasmic dynein and dynein-2 all represent potential candidates where structural and biophysical analysis allows one to consider similar in vitro screening based approaches to target core cargo recognition and autoregulatory mechanisms (38, 39, 42-44). Other candidates and mechanisms in all three families will surely emerge as studies continue to define the molecular underpinnings of these processes.

Finally, it is worth considering the potential of the kinesin-1-cargo interface itself as a drug target. Microtubule targeting agents (stabilizers and destabilizers) represent an important class of chemotherapeutics, but are limited by issues of both toxicity and resistance. Molecules that offer a mechanistically distinct approach to the modulation of microtubule dynamics are actively sought (45). It is conceivable that a molecule that bound the kinesin-1 cargo interface with both high affinity and selectivity, and elicited similar effects to kinesore, could represent such a drug. One might also consider whether manipulation of kinesin-1 activity could be advantageous in neurological conditions where axonal transport is impaired (46). Clearly therefore a structural understanding of the kinesore mechanism is imperative as this would facilitate rational design and phenotypic screening approaches.

Materials and Methods

Expression, purification and Terbium labelling of aiKLC2^{TPR}

His-KLC2 161-480 (aiKLC2^{TPR}) protein was expressed in BL21 E.coli, isolated by nickel affinity chromatography and further purified by size-exclusion chromatography in 500mM NaCl as previously described (25). 10ml of 100 µM (1 µmole) purified protein was dialysed overnight at 4°C into a labelling buffer comprising 100mM Na_2CO_3 and 150mM NaCl at pH 9.3. The protein was labelled with 100 µg (95 nmoles) of amine-reactive Terbium chelate (Lanthascreen, Thermofisher Scentific, PV3582) for 3 hours at room temperature on a rolling platform, giving a theoretical maximum labelling of approximately 1 Tb per 10 aiKLC2^{TPR}. The product of this reaction was subsequently centrifuged at 16,000 x g for 20 minutes and passed through 0.22

micron filter and further purified, removing any free label using a second round of size-exclusion chromatography on a 16⁄60 HiLoad Superdex 75 column (GE Healthcare), pooling all protein containing fractions (labelled and unlabelled). The presence of Tb with the characteristic 4 peak emission profile in the final pool was confirmed using a fluorimeter following excitation at 340nm. This mix of labelled and non-labelled aiKLC2 was then dialysed overnight at 4°C into 25mM HEPES (pH 7.5), 150mM NaCl, 5 mM β-ME buffer in preparation for use in the TR-FRET screen.

See SI materials and methods for additional materials and methods

Acknowledgments:

This work was funded by a Wellcome Trust R.C.D.F. to M.P.D (097316/Z/11/Z); Y.Y.Y is supported by a BBSRC project grant (BB/L006774/1, M.P.D. and R.A.S); K.P and M.P by UK MRC (MR/K015664/1); A.J.B by Asthma UK (09/029). We are grateful to Professor A. Hyman (Max-Planck Institute for Cell Biology and Genetics) for the gift HeLa-Kyoto cell lines, Dr. Rachel Gurrell (Pfizer Ltd, Cambridge, UK) for facilitating access to the Chemogenomics small molecule library, and Dr Simon Brayford (KCL) and the KCL Nikon Imaging Centre for assistance with microscopy. Professor Vladimir Gelfand (Northwestern University), Professor Ulrike Eggert (KCL) and Dr Anthony Roberts (Birkbeck) provided helpful discussions on the project and we thank Professor Anne Ridley (KCL) for critical reading of the manuscript.

References

1. Vale RD (2003) The molecular motor toolbox for intracellular transport. *Cell* 112(4):467–480.

2. Vale RD, Reese TS, Sheetz MP (1985) Identification of a novel force-generating protein, kinesin, involved in microtubule-based motility. *Cell* 42(1):39–50.

3. Verhey KJ, Hammond JW (2009) Traffic control: regulation of kinesin motors. *Nature Reviews Molecular Cell Biology* 10(11):765–777.

4. Fu M-M, Holzbaur ELF (2014) Integrated regulation of motor-driven organelle transport by scaffolding proteins. *Trends Cell Biol* 24(10):564–574.

5. Jolly AL, et al. (2010) Kinesin-1 heavy chain mediates microtubule sliding to drive changes in cell shape. *Proceedings of the National Academy of Sciences* 107(27):12151–12156.

6. Lu W, Gelfand VI (2017) Moonlighting Motors: Kinesin, Dynein, and Cell Polarity. *Trends Cell Biol*. doi:10.1016/j.tcb.2017.02.005.

7. Urrutia R, McNiven MA, Albanesi JP, Murphy DB, Kachar B (1991) Purified kinesin promotes vesicle motility and induces active sliding between microtubules in vitro. *Proceedings of the National Academy of Sciences* 88(15):6701–6705.

8. Andrews SB, Gallant PE, Leapman RD, Schnapp BJ, Reese TS (1993) Single kinesin molecules crossbridge microtubules in vitro. *Proceedings of the National Academy of Sciences* 90(14):6503–6507.

9. Straube A (2005) Conventional Kinesin Mediates Microtubule-Microtubule Interactions In Vivo. *Mol Biol Cell* 17(2):907–916.

10. Lu W, Lakonishok M, Gelfand VI (2015) Kinesin-1-powered microtubule sliding initiates axonal regeneration in Drosophila cultured neurons. *Mol Biol Cell* 26(7):1296–1307.

11. Pernigo S, Lamprecht A, Steiner RA, Dodding MP (2013) Structural Basis for Kinesin-1:Cargo Recognition. *Science* 340(6130):356–359.

12. Verhey KJ, et al. (2001) Cargo of kinesin identified as JIP scaffolding proteins and associated signaling molecules. *J Cell Biol* 152(5):959–970.

13. Blasius TL, Cai D, Jih GT, Toret CP, Verhey KJ (2007) Two binding partners cooperate to activate the molecular motor Kinesin-1. *J Cell Biol* 176(1):11–17.

14. Navone F, et al. (1992) Cloning and expression of a human kinesin heavy chain gene: interaction of the COOH-terminal domain with cytoplasmic microtubules in transfected CV-1 cells. *J Cell Biol* 117(6):1263–1275.

15. Seeger MA, Rice SE (2010) Microtubule-associated protein-like binding of the kinesin-1 tail to microtubules. *J Biol Chem* 285(11):8155–8162.

16. Kaan HYK, Hackney DD, Kozielski F (2011) The Structure of the Kinesin-1 Motor-Tail Complex Reveals the Mechanism of Autoinhibition. *Science* 333(6044):883–885.

17. Dietrich KA, et al. (2008) The kinesin-1 motor protein is regulated by a direct interaction of its head and tail. *Proc Natl Acad Sci USA* 105(26):8938–8943.

18. Hackney DD, Baek N, Snyder AC (2009) Half-Site Inhibition of Dimeric Kinesin Head Domains by Monomeric Tail Domains †. *Biochemistry* 48(15):3448–3456.

19. Hackney DD, Stock MF (2000) Kinesin's IAK tail domain inhibits initial microtubule-stimulated ADP release. *Nat Cell Biol* 2(5):257–260.

20. Friedman DS, Vale RD (1999) Single-molecule analysis of kinesin motility reveals regulation by the cargo-binding tail domain. *Nat Cell Biol* 1(5):293–297.

21. Stock MF, et al. (1999) Formation of the Compact Confomer of Kinesin Requires a COOH-terminal Heavy Chain Domain and Inhibits Microtubule-stimulated ATPase Activity. *J Biol Chem* 274(21):14617–14623.

22. Coy DL, Hancock WO, Wagenbach M, Howard J (1999) Kinesin's tail domain is an inhibitory regulator of the motor domain. *Nat Cell Biol* 1(5):288–292.

23. Verhey KJ, et al. (1998) Light chain-dependent regulation of Kinesin's interaction with microtubules. *J Cell Biol* 143(4):1053–1066.

24. Wong YL, Rice SE (2010) Kinesin's light chains inhibit the head- and microtubule-binding activity of its tail. *Proc Natl Acad Sci USA* 107(26):11781–11786.

25. Yip YY, et al. (2016) The light chains of kinesin-1 are autoinhibited. *Proc Natl Acad Sci USA* 113(9):2418–2423.

26. Kawano T, et al. (2012) A small peptide sequence is sufficient for initiating kinesin-1 activation through part of TPR region of KLC1. *Traffic* 13(6):834–848.

27. Dodding MP, Mitter R, Humphries AC, Way M (2011) A kinesin-1 binding motif in vaccinia virus that is widespread throughout the human genome. *EMBO J* 30(22):4523–4538.

28. Sanger A, et al. (2017) SKIP controls lysosome positioning using a composite kinesin-1 heavy and light chain-binding domain. *Journal of Cell Science* 130(9):1637–1651.

29. Lee TJ, Lee JW, Haynes EM, Eliceiri KW, Halloran MC (2017) The Kinesin Adaptor Calsyntenin-1 Organizes Microtubule Polarity and Regulates Dynamics during Sensory Axon Arbor Development. *Front Cell Neurosci* 11:391.

30. Nikolovska-Coleska Z, et al. (2004) Development and optimization of a binding assay for the XIAP BIR3 domain using fluorescence polarization. *Anal Biochem* 332(2):261–273.

31. Rosa-Ferreira C, Munro S (2011) Arl8 and SKIP act together to link lysosomes to kinesin-1. *Dev Cell* 21(6):1171–1178.

32. Oladipo A, Cowan A, Rodionov V (2007) Microtubule motor Ncd induces sliding of microtubules in vivo. *Mol Biol Cell* 18(9):3601–3606.

33. Maliga Z, et al. (2013) A genomic toolkit to investigate kinesin and myosin motor function in cells. *Nat Cell Biol* 15(3):325–334.

34. Tanaka Y, et al. (1998) Targeted disruption of mouse conventional kinesin heavy chain, kif5B, results in abnormal perinuclear clustering of mitochondria. *Cell* 93(7):1147–1158.

35. Essletzbichler P, et al. (2014) Megabase-scale deletion using CRISPR/Cas9 to generate a fully haploid human cell line. *Genome Res* 24(12):2059–2065.

36. Cross RA, McAinsh A (2014) Prime movers: the mechanochemistry of mitotic kinesins. *Nature Reviews Molecular Cell Biology* 15(4):257–271.

37. Ghiretti AE, et al. (2016) Activity-Dependent Regulation of Distinct Transport and Cytoskeletal Remodeling Functions of the Dendritic Kinesin KIF21B. *Neuron* 92(4):857–872.

38. Li J, Lu Q, Zhang M (2016) Structural Basis of Cargo Recognition by Unconventional Myosins in Cellular Trafficking. *Traffic* 17(8):822–838.

39. Zhang K, et al. (2017) Cryo-EM Reveals How Human Cytoplasmic Dynein Is Auto-inhibited and Activated. *Cell* 169(7):1303–1314.e18.

40. McKenney RJ, Huynh W, Tanenbaum ME, Bhabha G, Vale RD Activation of cytoplasmic dynein motility by dynactin-cargo adapter complexes. *sciencemagorg*.

41. Schlager MA, Hoang HT, Urnavicius L, Bullock SL, Carter AP (2014) In vitro reconstitution of a highly processive recombinant human dynein complex. *EMBO J*. doi:10.15252/embj.201488792.

42. Wei Z, Liu X, Yu C, Zhang M (2013) Structural basis of cargo recognitions for class V myosins. *Proc Natl Acad Sci USA* 110(28):11314–11319.

43. Toropova K, Mladenov M, Roberts AJ (2017) Intraflagellar transport dynein is autoinhibited by trapping of its mechanical and track-binding elements. - PubMed - NCBI. *Nat Struct Mol Biol* 24(5):461–468.

44. Talapatra SK, Harker B, Welburn JPI (2015) The C-terminal region of the motor protein MCAK controls its structure and activity through a conformational switch. *Elife* 4. doi:10.7554/eLife.06421.

45. Dumontet C, Jordan MA (2010) Microtubule-binding agents: a dynamic field of cancer therapeutics. *Nat Rev Drug Discov* 9(10):790–803.

46. Goldstein LSB (2012) Axonal transport and neurodegenerative disease: Can we see the elephant? *Progress in Neurobiology* 99(3):186–190.

Figure Legends

Fig. 1. Identification of kinesore as a small molecule inhibitor of KLC-cargo interaction.
(A) Scheme showing three stage screening strategy for small molecule inhibitors of the aiKLC2^{TPR} – SKIP^{WD} (SEQ:STNLEWDDSAI) interaction and the chemical structure of kinesore. **(B)** Western blot of GST-pull-down experiment showing that the interaction between bacterially expressed GST-SKIP(1-310) and HA-KLC2 expressed in mammalian cell extracts is inhibited by kinesore. All pulldown lanes, including controls were performed in the presence of 0.1% DMSO. Graph shows quantification of 3 independent experiments. Error ± SEM. **(C)** FP experiment titrating increasing concentrations of kinesore into a aiKLC2^{TPR}:SKIP^{WD} complex showing that kinesore inhibits the interaction. Data are derived from 3 replicates and are representative of 3 independent experiments. Error ± SEM.

Fig. 2. Kinesore induces the remodeling of the microtubule network. (A) Representative maximum intensity projection immunofluorescence images acquired using a Ziess 880 Airyscan microscope of HeLa cells treated with 50μM kinesore or vehicle control (0.1% DMSO) for 1 hour. Cells were immunostained for β-tubulin (green) and LAMP1 (magenta). **(B,C,D)** Stills derived from supplementary movie 1 showing representative dynamics of GFP-tubulin in live HeLa cells treated with 50μM kinesore for one hour. Numbering denotes time in seconds from start of the still sequence. **(E)** Pseudocoloured spinning disk confocal microscopy projection images from the first 5 frames (20sec) of supplementary movies 2 and 3, showing dynamics of EB3-RFP in control and kinesore treated HeLa cells (Scale bars: 10 μm).

Fig. 3. Kinesore induced remodeling of the microtubule network is dependent on kinesin-1
(A) Representative maximum intensity projection confocal immunofluorescence images showing HeLa cells transfected with mCit-KHC (pseudocoloured red) and HA-KLC (pseudocoloured blue) treated with 50μM kinesore (right) or vehicle control (left) (0.1% DMSO) for 1 hour. Note the change in localisation of kinesin-1 (KHC/KLC) and formation of microtubule rich projections in kinesore treated cells. Images are representative of 3 independent experiments (Scale bar: 10 μm.). **(B)** Structured illumination images of kinesore treated cells as in **(A)** (Scale bar: 5 μm.). **(C)** Representative immunofluorescence images of HAP1 cells (wild type or Kif5B knockout) treated with 50μM kinesore or vehicle control (0.1% DMSO) for 1 hour and stained for β-tubulin (green) or DNA (Hoechst, blue). Microtubule rich projections induced by kinesore are strongly suppressed by knockout of Kif5B (Scale bar: 10 μm.). Western blot shows whole cell extracts of WT or Kif5B knockout HAP1 cells probed with either a Kif5B specific polyclonal antibody or a pan-KHC monoclonal antibody (SUK4)**.**

Fig. 4. Kinesore induces the cargo-driven KLC conformational switch.
(A) Schematic showing KLC2 FRET biosensor with an N-terminal eGFP and a C-terminal HaloTag that allows covalent coupling of TMR. On the left, the autoinhibitory interaction mediated by the light chain LFP motif is indicated (25). Right shows a representation of the change in conformation to the low FRET state induced by the co-expression of the W-acidic cargo CSTN1. **(B)** Multiphoton fluorescent lifetime images of FRET between GFP and TMR-HaloTag in cells transfected with HA-KHC and GFP-KLC2-Halo biosensor and either co-transfected with CSTN(879-971)(cargo) or treated with 50μM kinesore for 1 hour. "GFP int." are multiphoton GFP intensity images, whereas lifetime image refers to the fluorescence lifetime of GFP (τ) and is represented by a pseudocolor scale. In these images, a reduction in lifetime (change in color from blue to red) indicates FRET and therefore close association of GFP and TMR-HaloTag. Graphs show data from 12 cells from 2 independent experiments expressed as FRET efficiency (Scale bar: 10 μm.). FRET is significantly reduced by either cargo co-transfection or 1 hr kinesore treatment. Error bars are ± SEM. ***$P < 0.001$ determined using one-way ANOVA and comparing to control.

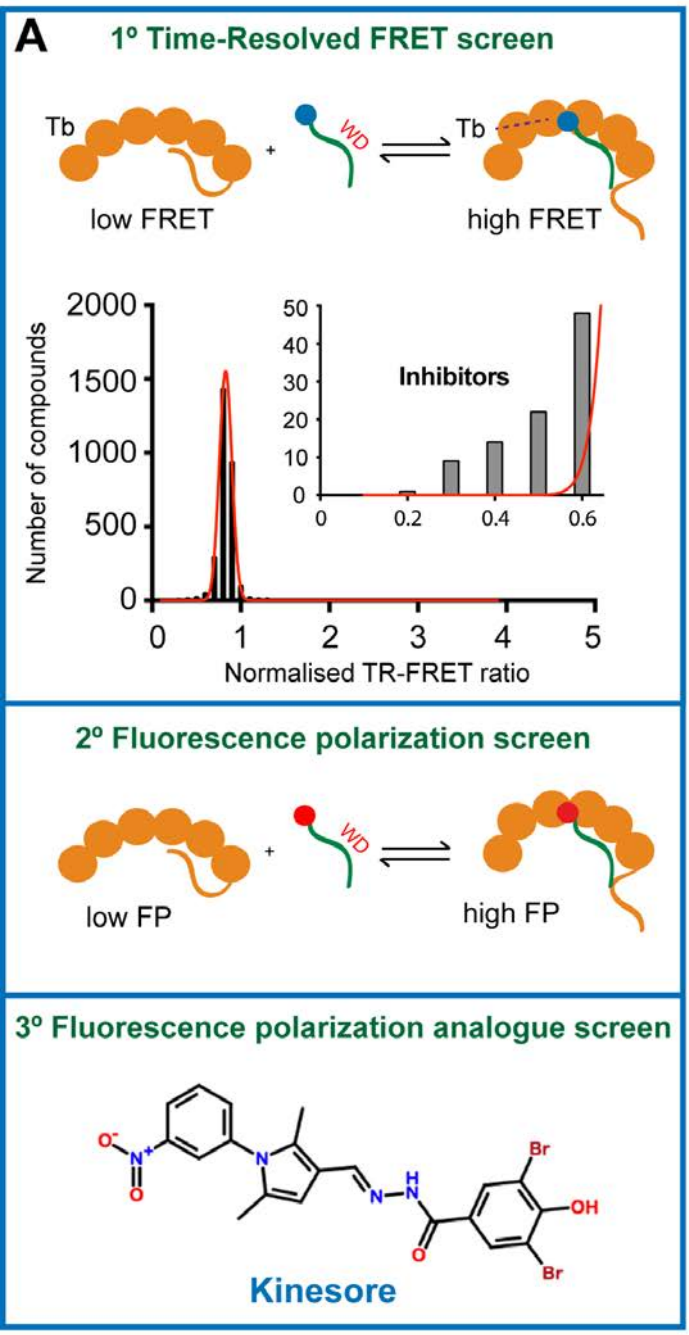
A
1º Time-Resolved FRET screen
Tb
WD
Tb
low FRET
high FRET
Number of compounds
Normalised TR-FRET ratio
Inhibitors
2º Fluorescence polarization screen
WD
low FP
high FP
3º Fluorescence polarization analogue screen
Kinesore

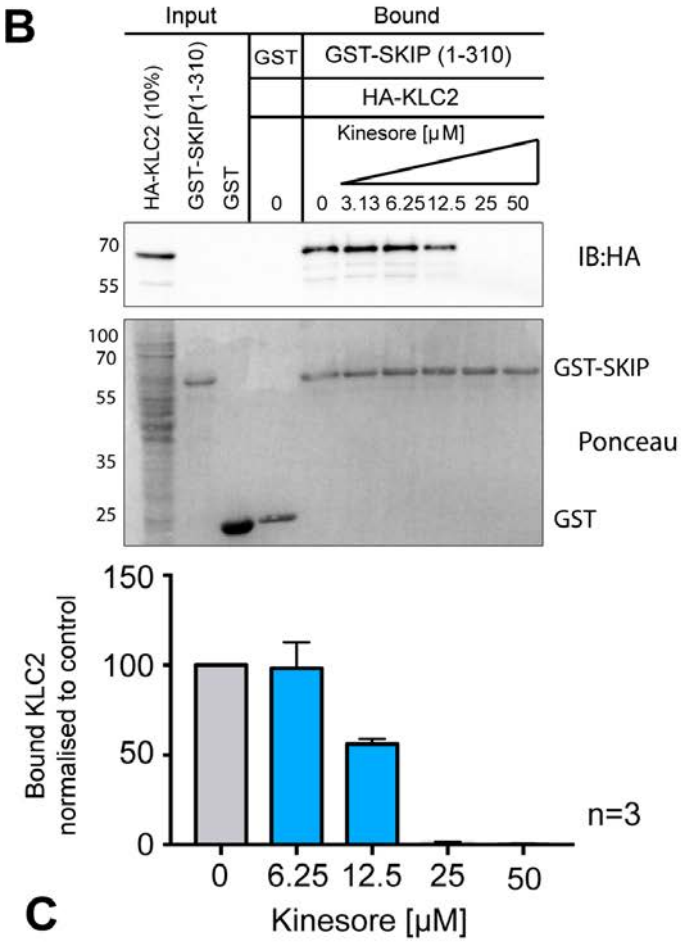
B
Input
Bound
GST
GST-SKIP (1-310)
HA-KLC2
Kinesore [μM]
HA-KLC2 (10%)
GST-SKIP(1-310)
GST
0
0 3.13 6.25 12.5 25 50
IB:HA
GST-SKIP
Ponceau
GST
Bound KLC2 normalised to control
n=3
Kinesore [μM]

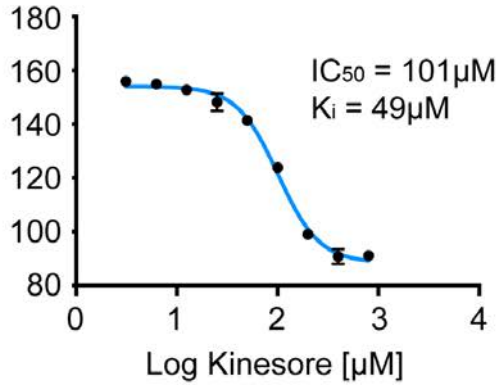
C
IC50 = 101μM
Ki = 49μM
Log Kinesore [μM]

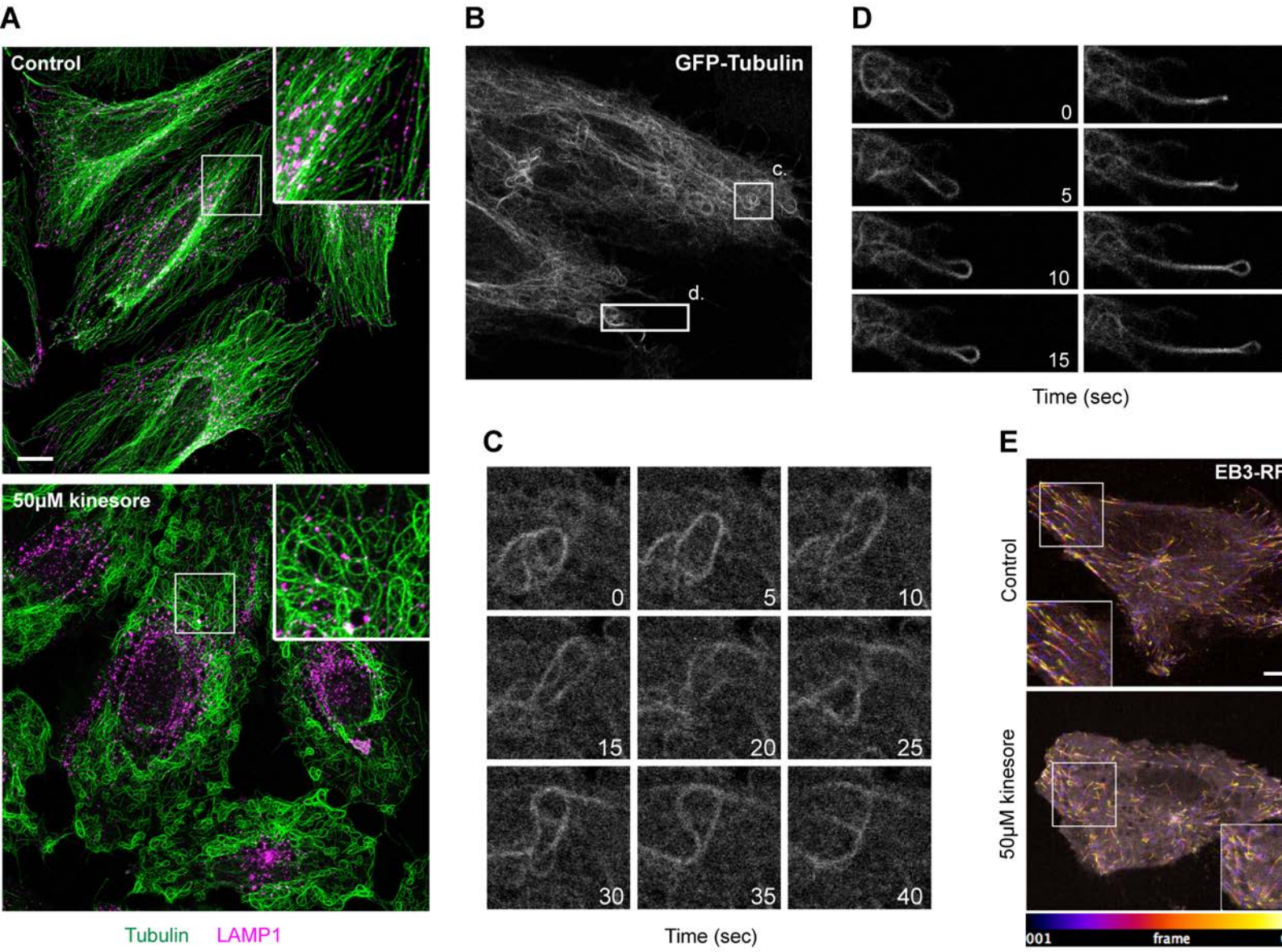
A
Control
50μM kinesore
Tubulin
LAMP1
B
GFP-Tubulin
c.
d.
C
0
5
10
15
20
25
30
35
40
Time (sec)
D
0
5
10
15
Time (sec)
E
EB3-RF
Control
50μM kinesore
001
frame

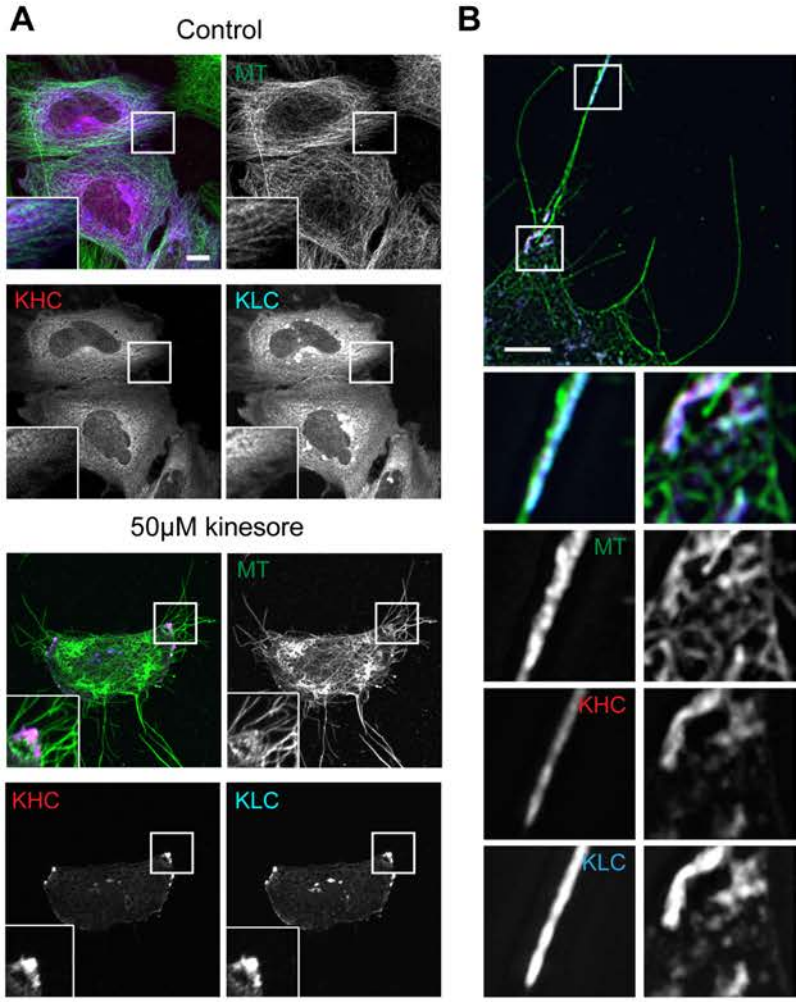
A
Control
MT
KHC
KLC
50μM kinesore
MT
KHC
KLC
B
MT
KHC
KLC

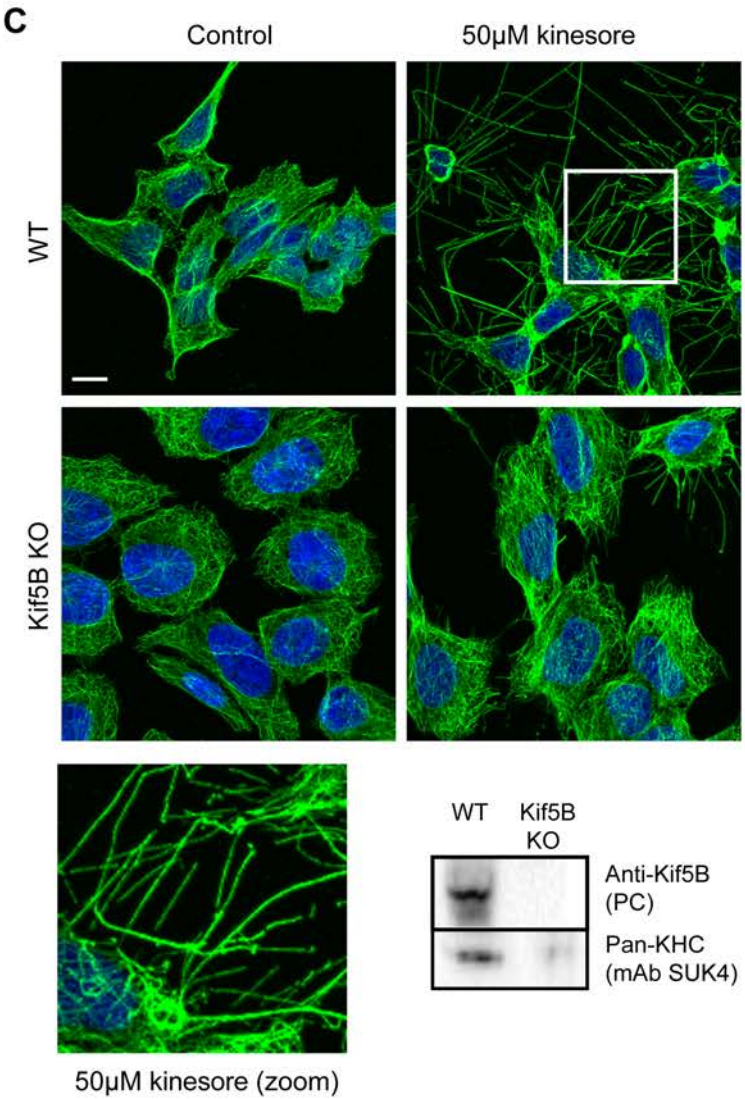
C
Control
50μM kinesore
WT
Kif5B KO
50μM kinesore (zoom)
WT
Kif5B KO
Anti-Kif5B (PC)
Pan-KHC (mAb SUK4)

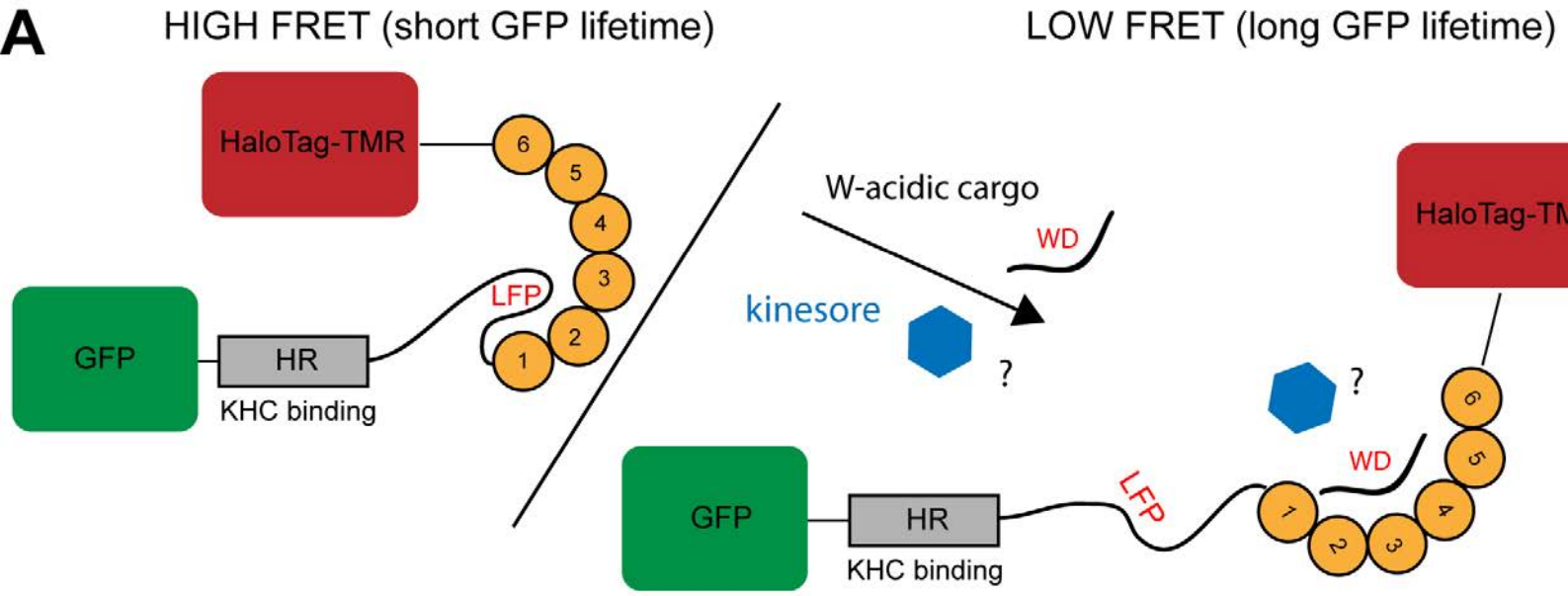
A
HIGH FRET (short GFP lifetime)
LOW FRET (long GFP lifetime)
HaloTag-TMR
6
5
4
3
2
1
LFP
GFP
HR
KHC binding
W-acidic cargo
WD
kinesore
?
?
HaloTag-TM
WD
LFP
GFP
HR
KHC binding
6
5
4
3
2
1

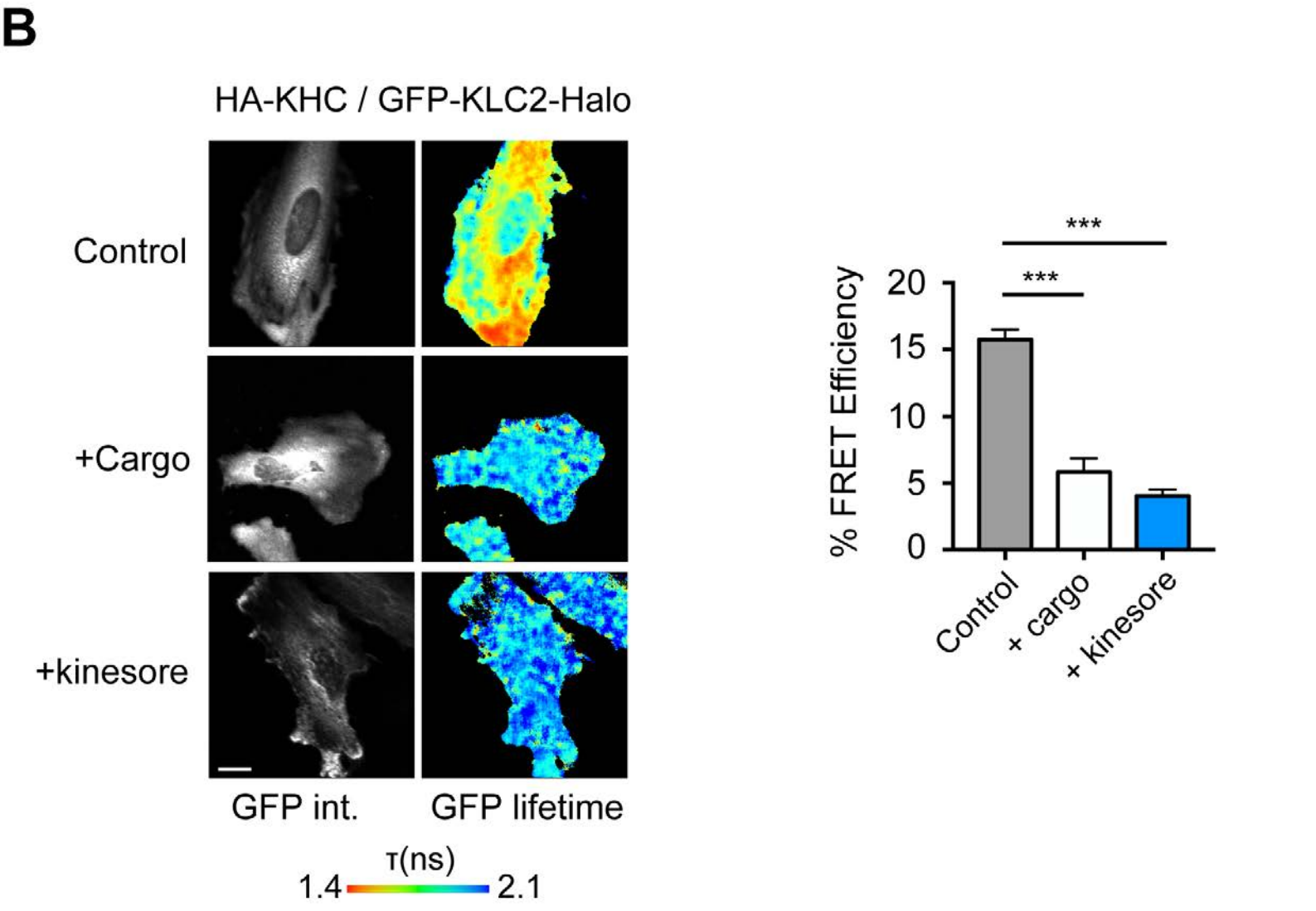
B
HA-KHC / GFP-KLC2-Halo
Control
+Cargo
+kinesore
GFP int.
GFP lifetime
τ(ns)
1.4
2.1
***
***
% FRET Efficiency
20
15
10
5
0
Control
+ cargo
+ kinesore

SI Materials and Methods

TR-FRET assay for a the primary screen of the 2908 compound Pfizer Chemogenomics small molecule library

The screen was carried out using non-binding coated 384-well plates with flat bottomed wells (Corning, 781900). 250nl of 2,908 compounds at 4mM in DMSO, or DMSO only controls, were supplied prealiquoted in duplicate wells on the same plate. A premade master reaction mix comprising 20µl of 8 µM Tb-aiKLC2^{TPR}, 10µM Alexa647-SKIP^{WD} (95% unlabeled peptide, 5% labeled, amino terminally conjugated, sequence STNLEWDDSAI, Biosynthesis Inc, Lewisville) in 25mM HEPES (pH 7.5), 150mM NaCl, 5mM β-ME, was added to each well (giving a final DMSO concentration of 1.25% v/v and compound concentration of 49.4µM). Plates were incubated at room temperature for 30 minutes and subsequently analysed using a Artemis TR-FRET K-101 plate reader (Kyoritsu Radio Co., Ltd.) at an excitation wavelength of 340nm, measuring FRET as a ratio of 665 nm (acceptor) to 620nm (donor) emission intensity, with a time delay of 100 µsec following excitation. TR-FRET ratio was normalised to in plate DMSO controls. Compounds that elicited a decrease in TR-FRET ratio that fell outside of a fitting of a normal distribution to the data (50 compounds) were selected for further analysis. Compounds with inconsistent duplicates were disregarded**.**

FP assay for secondary and tertiary screens

Fluorescence polarisation (FP) experiments for the purpose of secondary screening were performed in duplicate in black non-binding 96-well plates with flat bottomed wells (Corning, 655900). 50 compounds identified from the initial TR-FRET assay were supplied prealiquoted on plates in a 1µl volume at a concentrations of 0.25mM – 4mM, and tested in a 2 fold dilution series, giving final reaction concentrations ranging from 3.5 – 57µM. 70µl of a master mix solution containing 8µM non-labelled aiKLC2^{TPR} produced as described above, 150nM TAMRA conjugated *SKIP*^{WD} peptide (11). 25mM HEPES (pH 7.5), 150mM NaCl, 5mM β-ME were added to each well (giving a final DMSO concentration of 1.4%) per reaction and mixed by gentle pipetting. mP values for

control reactions were at approximately 60% of those obtained with a saturating amount of protein (25). Plates were incubated at room temperature for 30 minutes and subsequently analysed using a POLARstar Omega plate reader (BMG Labtech), using the Omega software at an excitation wavelength of 540nm and an emission wavelength of 590nm. For each independent 96-well plate reading the gain of the parallel and perpendicular channel was adjusted according to a 150 nM SKIP-TAMRA peptide only control (25 mM HEPES [pH 7.5], 150 mM NaCl, 5 mM β-ME, 1.5 % v/v DMSO) to target 100mP. Compounds identified as causing a concentration dependent decrease in FP (8 compounds, 0.28% of initial library) were selected for further analysis by GST-pull down analysis and optimised FP conditions (as above with 100µl total volume). This data was used to inform a small-scale targeted screen of compounds selected from the Hit2Lead library from Chembridge, which were analysed in the same way. Kinesore was identified as 3,5-dibromo-N'-{[2,5-dimethyl-1-(3-nitrophenyl)-1H-pyrrol-3-yl]methylene}-4-hydroxybenzohydrazide, compound number 6233307. The concentration-dependent decrease in FP signal due to the addition of compound was fitted using a four-parameter dose-response curve without constraints to derive IC_{50} and apparent Ki was determined as previously described by Nikolovska-Coleska *et al*. (32). Data was analysed using GraphPad Prism version 7.00 (GraphPad Software, La Jolla California, USA).

Kinesore treatment of cells

Kinesore stocks were prepared by solubilisation of dry powder at a concentration of 50mM in 100% DMSO and stored at -20°C prior to use. All treatments were carried out in Ringer's buffer (155mM Nacl, 5mM KCl, 2mM CaCl2, 1mM MgCl2, 2mM NaH2PO4, 10mM glucose, 10mM HEPES (pH 7.4)). Final concentration of DMSO in 50µM treatment was therefore 0.1%. Vehicle control experiments refer to cells treated with 0.1% DMSO in Ringers buffer. For lower concentration treatments, stocks were first diluted in DMSO to yield a 1000X solution that was subsequently added to Ringers buffer.

Plasmids, antibodies and cells

All bacterial and mammalian expression plasmids used in this study have been described previously (11,25). FRET biosensor plasmids are described in (25). The SUK4 monoclonal antibody was supplied by the Developmental Studies Hybridoma Bank. Anti-HA monoclonal antibody (HA-7) used for western blot, anti-HA polyclonal antibody (H6908) used for IF, and anti-β-tubulin (B-5-1-2) were supplied by Sigma-Aldrich. HAP1 cells were supplied by Horizon Discovery.

GST-Pull down from cell extracts

GST-SKIP(1-310) was expressed and purified from *E.coli* as described previously (28). HEK 293T cells expressing transiently transfected HA-KLC2 were harvested in 1mL lysis buffer (25 mM HEPES pH 7.5, 150 mM NaCl, 0.1% NP-40, 0.1% Triton-X 100 containing a protease inhibitor cocktail (Roche)). Lysates were incubated on ice for 10 minutes prior to centrifugation at 13000g for 10 min at 4°C. The resulting supernatant was pre-incubated with the corresponding concentration of kinesore for 30 minutes in 0.1% DMSO (from 1000X stocks, in 100% DMSO) or without kinesore with 0.1% DMSO (lane 5), and subsequently incubated for 1 ½ hours with the indicated GST-fusion protein (0.5µmol of protein per reaction, unless otherwise indicated) bound to 20µl glutathione sepharose beads. Beads were washed four times and boiled in 60µl SDS loading buffer. 20µl samples were separated on SDS-PAGE gels, transferred onto PVDF membrane, blocked in 5% milk in TBS-T (20mM Tris, 0.25M NaCl, 0.1% Tween-20, pH 7.5 with HCl), and probed with the indicated primary antibodies followed by detection with HRP conjugated secondary antibodies. Blots were developed with an ECL kit (Biorad) and chemiluminescent signal detected and quantified using a Bio-Rad XR system and ImageLab software.

Immunofluoresence and live-cell imaging

2 x 10^5 cells were plated onto fibronectin coated coverslips in 6-well plates and transfected, where indicated the plasmid DNA 16 hours prior to analysis. Cells treated with kinesore as indicated, and fixed for 5 minutes with −20°C methanol before blocking and probing with primary and secondary antibodies (Alexa 488, 568 and 633 conjugated anti-mouse or anti-rabbit secondary antibodies, Thermoscientific). Confocal images were

collected using a Nikon A1 system with a 40x or 60x objective running NIS Elements and are presented as maximum intensity projections where indicated. Super-resolution imaging was performed using an N-SIM Super resolution system with a 100x objective lens and images presented are maximum intensity projections. For live- cell imaging, 1x 10^5 the indicated cells were plated and transfected in fibronectin coated 35 mm Mattek dishes, and were imaged at a either using an inverted Nikon A1 confocal system with a 100x objective lens (GFP-tubulin) or an inverted CSU- X1 Spinning Disk Confocal system (EB3-RFP) with an Andor Ixon3 EM- CCD camera and a 60x objective lens both equipped with temperature and CO_2 control and running NIS Elements. Movies were processed using NIS elements and Image J. Figures were assembled using Image J in conjunction with Adobe Photoshop and Illustrator packages (Adobe, CA, USA). Spectrum projection images in figure 2E were generated using the Time-lapse colour coder Image J plugin.

FRET/FLIM Sample Preparation and Data Acquisition.

FRET biosensor studies were carried out as previously described, using a updated microscope set up (25). Briefly, 1×10^4 HeLa cells were seeded onto 13-mm fibronectin coated coverslips in 24-well plates. Cells were transfected with plasmids expressing GFP-KLC2-HaloTag and HA-KHC, with or without myc-CSTN1 (869–971). After 6 h posttransfection, medium was replaced with fresh medium containing HaloTag TMRDirect ligand (Promega) at a 1:1,000 dilution according to manufacturer's instructions. After an overnight incubation, cells were fixed in 4% paraformaldehyde and permeabilized in 0.2% (wt/vol) Triton X-100 in PBS. After quenching with 1 mg/mL sodium borohydride in PBS for 10 min at room temperature (RT), cells were washed in PBS and mounted in Mowiol containing 2.5% (wt/vol) Dabco (Sigma-Aldrich). Time domain FLIM was performed with a multiphoton microscope system (Ti Eclipse microscope; Nikon). Fluorescence lifetime imaging capability was provided by time-correlated single-photon counting electronics (SPC-830) on DCC-100 control (both Becker & Hickl). A 40x objective was used throughout (Plan Fluor N.A. 1.3; DIC H, WD 0.2; Nikon), and data were collected at 515 ± 20 nm through a bandpass filter. Acquisition times of the order of 250 s at a low 900-nm excitation laser power (MaiTai,

DeepSee; Spectra-Physics) were used to achieve sufficient photon statistics for fitting, while avoiding either pulse pile up or significant photobleaching. Corresponding widefield fluorescent images were acquired for donor (GFP) and acceptor (RFP) channels (DS-Qi1Mc camera; Nikon). Lifetime raw data were analysed with TRI2 software (Paul Barber) and histogram data are plotted as mean FRET efficiency from specified numbers of cells per sample over two experiments. Lifetime images of example cells are presented using a pseudocolor scale, whereby blue depicts normal GFP lifetime (no FRET) and red depicts lower GFP lifetime (areas of high FRET).

Microtubule polymerisation assay

In vitro microtubule polymerisation assay was carried out using the Tubulin Polymerization Assay Kit (Cytoskeleton, Inc.) according to the manufacturer's protocol using a POLARstar Omega (BMG Labtech) plate reader, with kinesore at 10μM or a 0.1% DMSO control. Data are presented as background subtracted from t=0 timepoint and are mean of 2 independent experiments.

Cellular microtubule sedimentation assay

This assay was adapted from the Cytoskeleton Inc Microtubule/Tubulin In Vivo Assay Biochem Kit and was previously described in (28). Briefly, 2×10^6 HeLa-Kyoto cells expressing GFP-Kif5B were plated onto a 10 cm dish. Cells were lysed at 24 h post plating, and 1 hour post kinesore treatment, in 3 ml of MT stabilization buffer [100mM PIPES pH 6.9, 5 mM MgCl2, 1 mM EGTA, 30% (v/v) glycerol, 0.1% (v/v) Nonidet P40, 0.1% (v/v) Triton X-100, 0.1% (v/v) Tween-20, 0.1% (v/v) β-mercaptoethanol, 100 μM GTP] supplemented with protease inhibitors. 1ml of lysate was subjected to ultracentrifugation to pellet intact MTs (100,000 g for 30 min at 37°C). Supernatant containing the soluble tubulin fraction was removed into a microfuge tube with 5× SDS sample buffer; 50μM 1× sample buffer was added to the pellet fraction. 20 μl of each fraction were separated by SDS-PAGE electrophoresis, immunoblotted and analysed using Biorad Imagelab software.

Supplementary Figure Legends

Fig. S1.

Time course of kinesore induced microtubule reorganization in fixed HeLa cells. Time of treatment of kinesore at 50μM (in minutes) is indicated in the bottom right of each panel. Nuclei are labeled with Hoescht (blue), microtubules (green) are immunostained. Images are representative of 3 independent experiments (Scale bars: 10 μm.).

Fig. S2

Concentration dependence and effect of washout on kinesore phenotype. (A) Concentration dependence of kinesore phenotype. HeLa cells were treated for one hour with the indicated concentration of compound, fixed and immunostained for tubulin (green) and LAMP1 (red). Nuclei are stained with Hoechst (blue) (B) Two hour washout experiment for cells treated for one hour with the indicated concentration of kinesore. The radial microtubule array is reestablished. (Scale bars: 10 μm.).

Fig. S3

Nocodazole disrupts kinesore induced loops and bundles. HeLa cells were treated with (left) DMSO control for 60 minutes, followed by 10 μM nocodazole, (middle) 50μM kinesore for 90 mins, or (right) 50μM kinesore for 60 minutes followed by 10 μM nocodazole + 50μM kinesore for 30 minutes.

Fig. S4

Effect of kinesore on the microtubule network in a panel of normal and cancer cell lines. The indicated cells were treated with vehicle or kinesore for 1 hour, methanol fixed and immunostained for tubulin (green). Nuclei are labeled with Hoescht (blue) (Scale bars: 10 μm.)

Fig. S5

Effect of kinesore on the in vitro polymerization and depolymerization kinetics of tubulin. (A) In vitro tubulin polymerization assays performed with 10μM kinesore or vehicle control (0.1% DMSO) and extent of tubulin assembly was monitored by absorbance at 340nm. Data are derived from 2 independent experiments and error bars show ±SEM. A control curve from assays performed in the presence of 10μM taxol is shown for comparison. (B) Results from a separate

experiment where microtubules were polymerized in the presence of DMSO control or kinesore until maximum absorbance was reached. Plates were then incubated at 4°C for 2 minute intervals and absorbance measured. This was repeated until absorbance decreased to a plateau.

Fig. S6

Effect of kinesore on the localization of kinesin-1 subunits, fused to GFP, stably expressed under control of their endogenous promoter. The indicated cells were treated with vehicle or kinesore for 1 hour, methanol fixed and immunostained for tubulin (green). GFP (C-LAP/N-FLAP) kinesin-1 subunits are shown in magenta. (Scale bars: 10 μm.).

Fig. S7

Effect of kinesore on association of GFP-KIf5B (N-FLAP) association with microtubules. Cells were lysed in a microtubule stabilizing buffer following 1 hour treatment with kinesore at 50μM and lysates were subjected to centrifugation to pellet polymerised microtubules and associated proteins. Pellets and supernatant fractions were analysed by western blot for GFP (Kif5B/KHC) and tubulin. Graph shows quantification of protein in pellet fractions from 3 independent experiments, following normalisation to control. Error bars show ±SEM. * indicates $p<0.05$ obtained using 2-tailed t-test. ns = not significant.

Movie S1

Confocal image sequence at 5 second intervals for 9 minutes of HeLa cells stably expressing GFP-tubulin and treated with 50μM kinesore for 1 hour. Image sequence begins after 1 hour of treatment.

Movie S2 and S3

Spinning disk confocal image sequences at 5 second intervals for 2 minutes of HeLa cells stably expressing EB3-RFP in control conditions (S1) or treated with 50μM kinesore for 1 hour (S2).

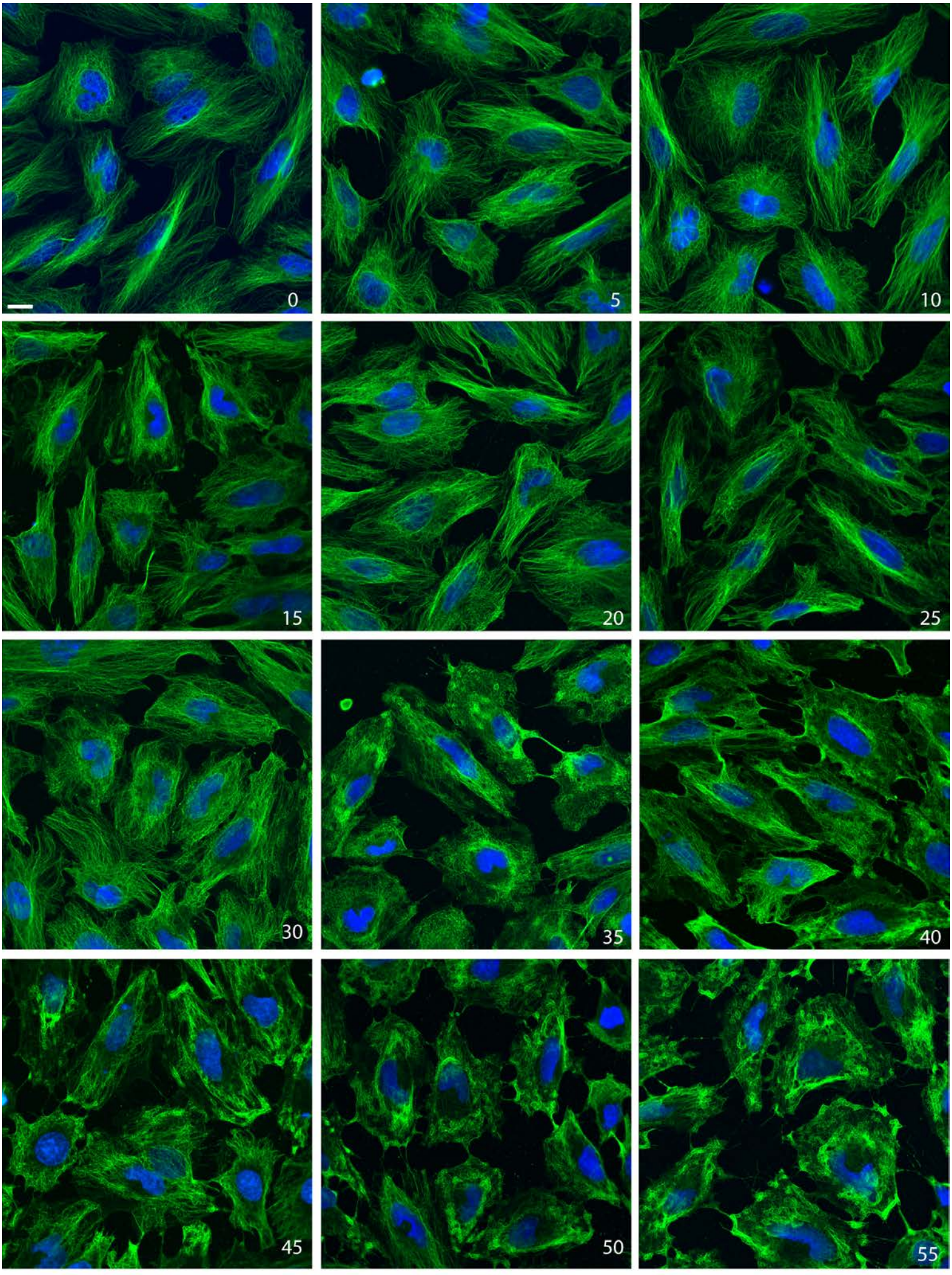

Fig. S1

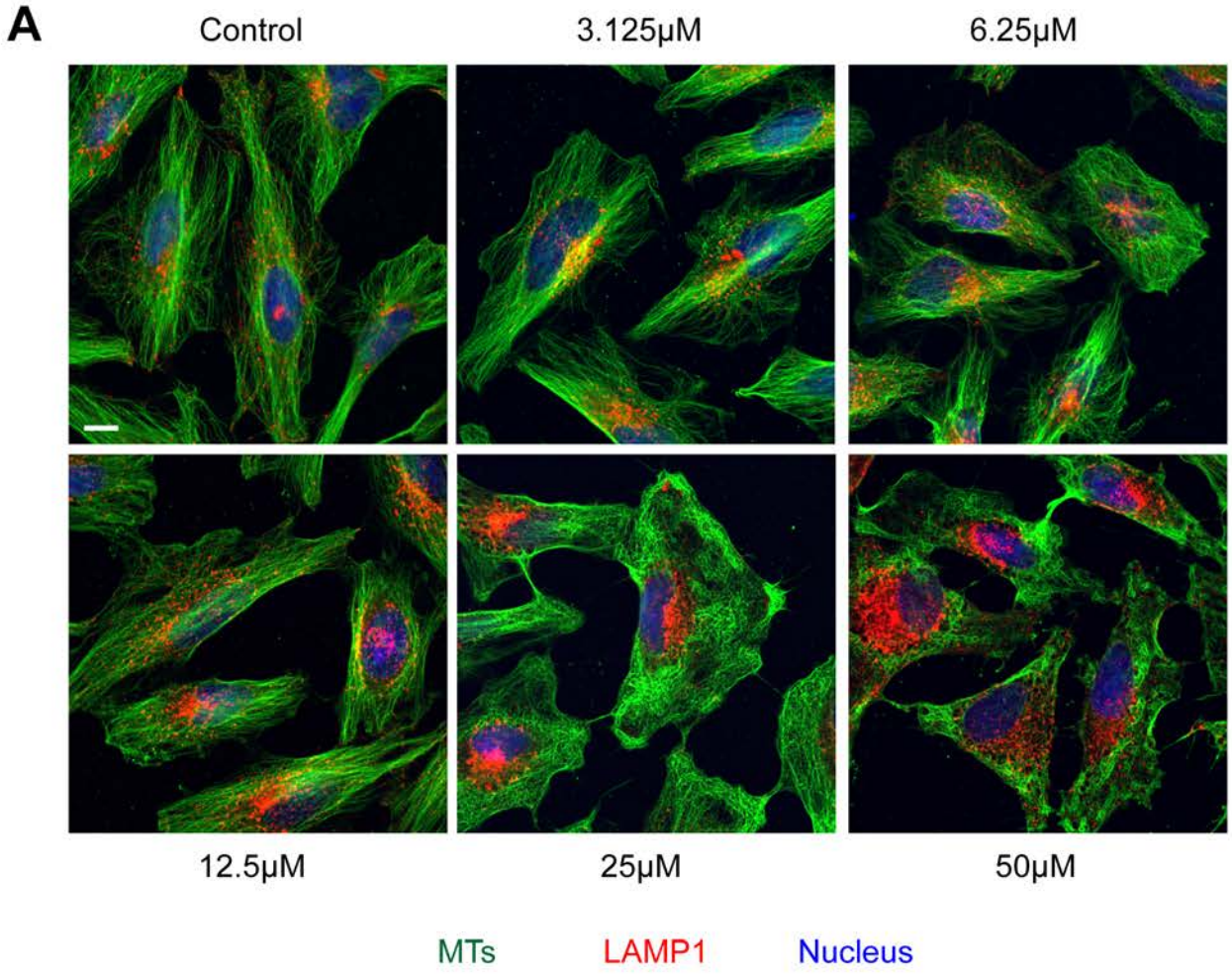
A
Control
3.125μM
6.25μM
12.5μM
25μM
50μM
MTs
LAMP1
Nucleus

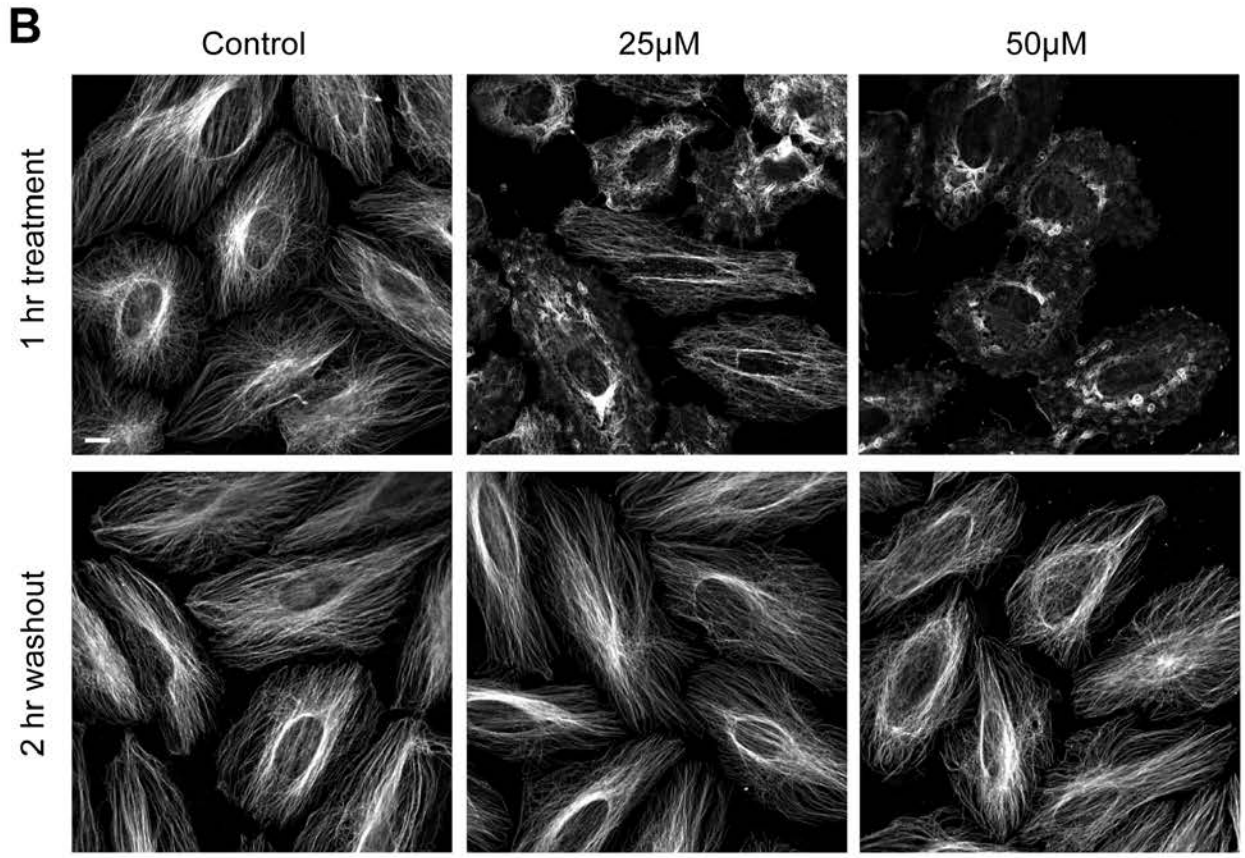
B
Control
25μM
50μM
1 hr treatment
2 hr washout

Fig. S2

i. 0.1% DMSO Control 60 mins
ii. Nocodazole at 10μM for 30 mins

Kinesore at 50μM for 90 mins

i. Kinesore at 50μM for 60 mins
ii. Kinesore at 50μM + Nocodazole 10μM for 30 mins

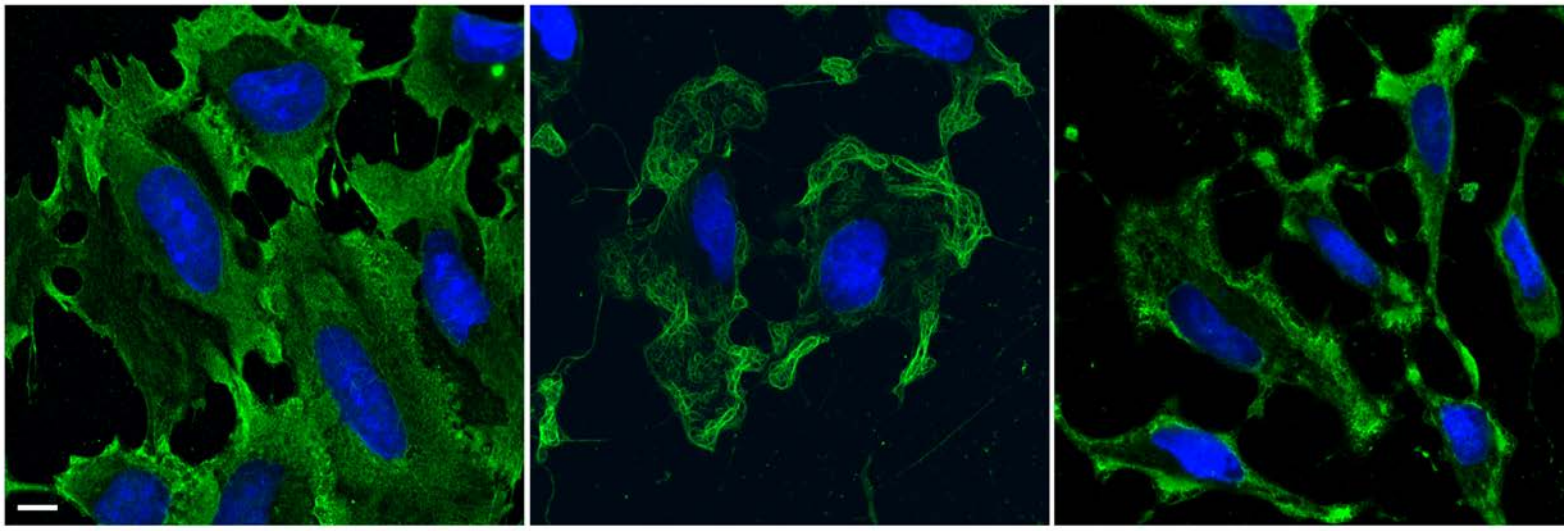

Fig. S3

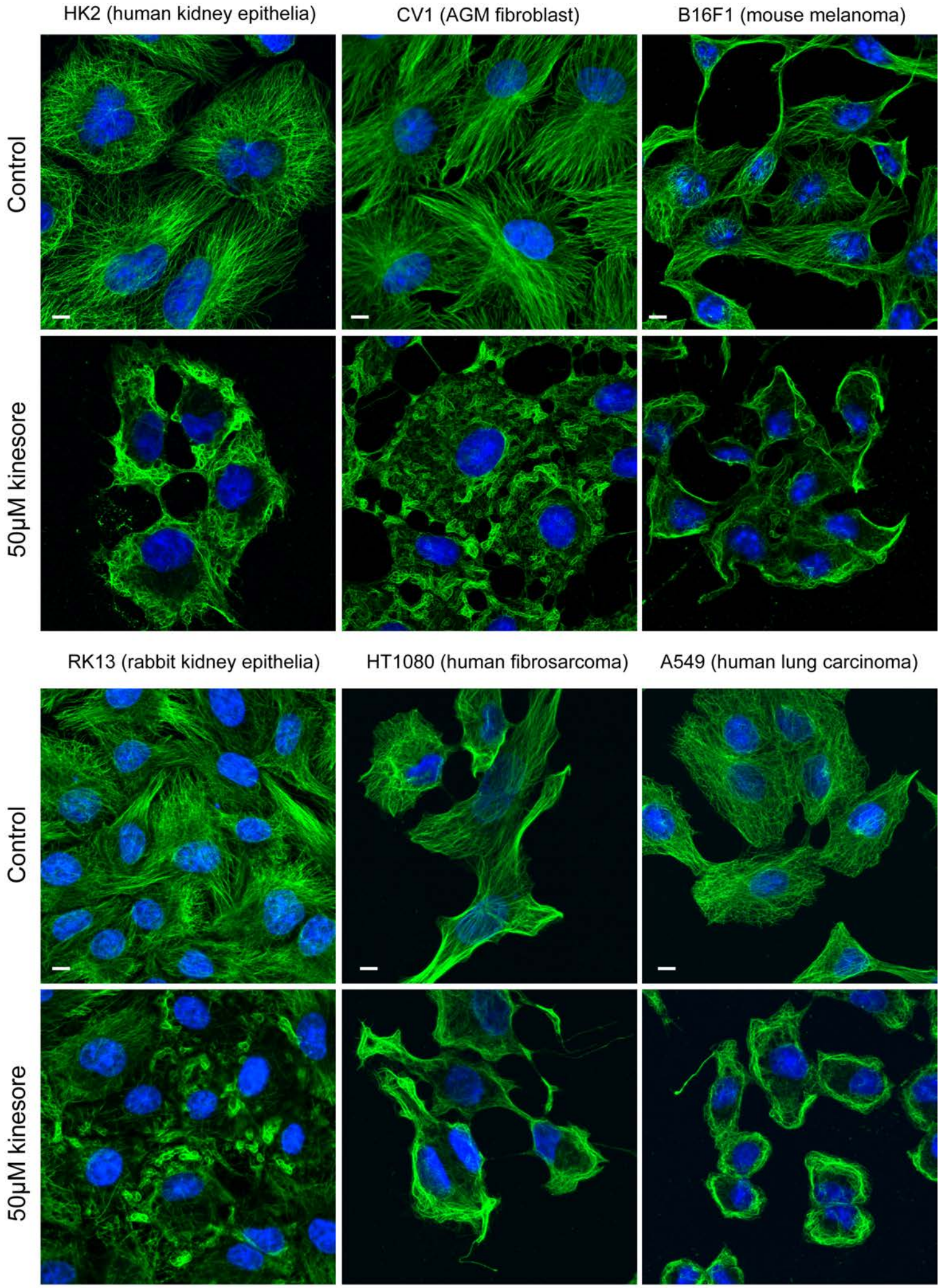
HK2 (human kidney epithelia)
CV1 (AGM fibroblast)
B16F1 (mouse melanoma)
Control
50μM kinesore
RK13 (rabbit kidney epithelia)
HT1080 (human fibrosarcoma)
A549 (human lung carcinoma)
Control
50μM kinesore

Fig. S4

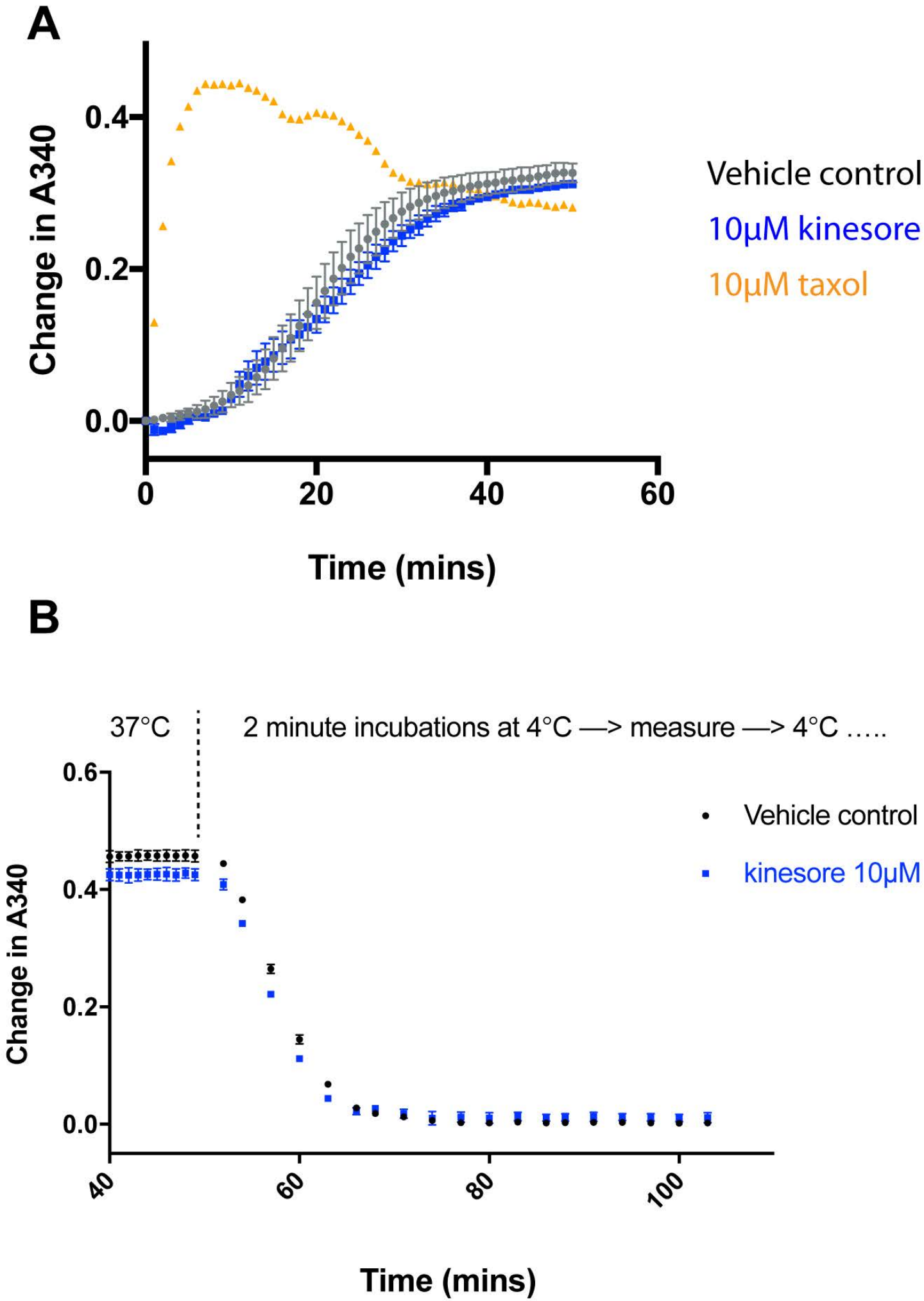
A
Change in A340
0.4
0.2
0.0
0
20
40
60
Time (mins)
Vehicle control
10μM kinesore
10μM taxol
B
37°C
2 minute incubations at 4°C —> measure —> 4°C …..
Change in A340
0.6
0.4
0.2
0.0
40
60
80
100
Time (mins)
Vehicle control
kinesore 10μM

Fig. S5

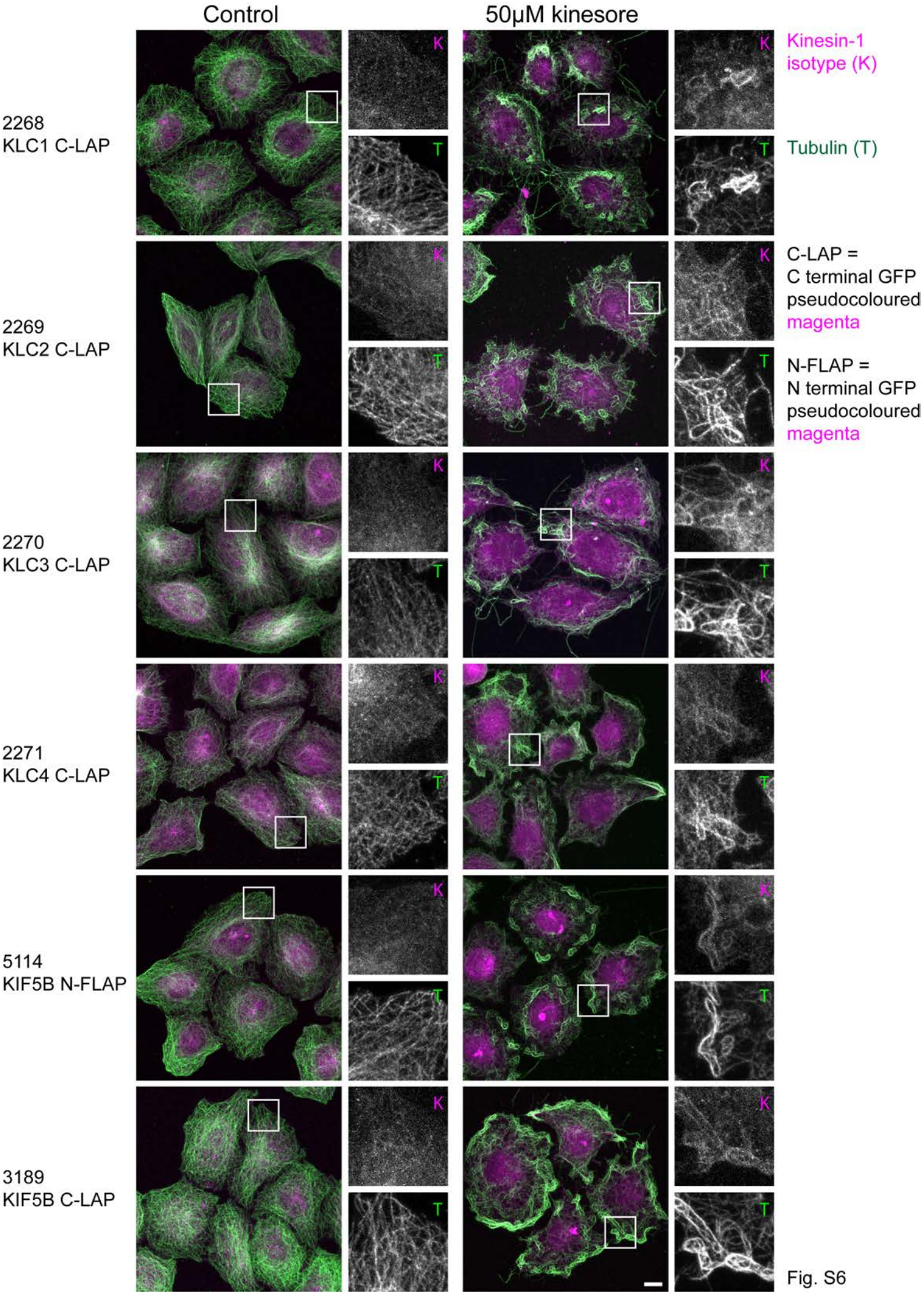
Control
50μM kinesore
2268
KLC1 C-LAP
2269
KLC2 C-LAP
2270
KLC3 C-LAP
2271
KLC4 C-LAP
5114
KIF5B N-FLAP
3189
KIF5B C-LAP
K
T
Kinesin-1
isotype (K)
Tubulin (T)
C-LAP =
C terminal GFP
pseudocoloured
magenta
N-FLAP =
N terminal GFP
pseudocoloured
magenta

Fig. S6

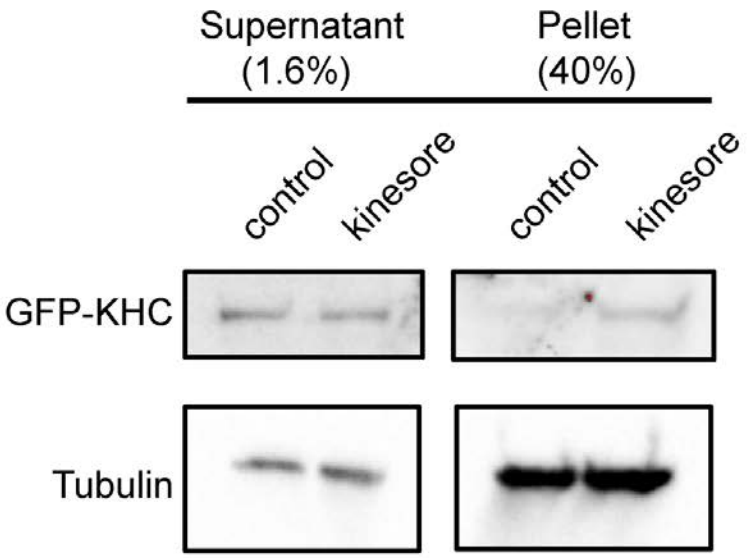

Vehicle control (0.1% DMSO)
or kinesore treatment for 1 hour at 50 μM.

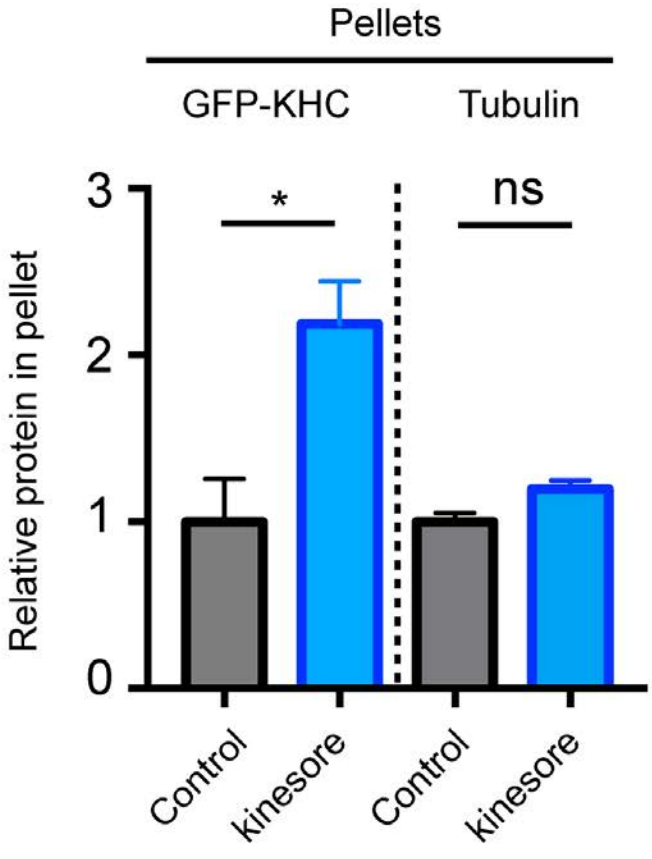

Fig. S7